Study of the highly excited states of antiprotonic helium atoms

(   )

The antiprotonic helium atom $\overline{\mathrm{p}}\mathrm{He}^+$ is a Coulomb three-body system consisting of an antiproton, an electron in the ground state, and a helium nucleus. The antiproton occupies a Rydberg state with large principal ($n \sim 38$) and orbital angular momentum ($l \sim n-1$) quantum numbers (see Figure 1). These states are metastable, i.e., they have microsecond-scale lifetimes against antiproton annihilations. The atomic transition frequencies of $\overline{\mathrm{p}}\mathrm{He}^+$ have been recently measured by laser spectroscopy with fractional precisions of $(2.3-5) \times 10^{-9}$ [1]. Comparisons between the measured frequencies and three-body quantum electrodynamics (QED) calculations have yielded an antiproton-to-electron mass ratio as $M_{\overline{\mathrm{p}}}/m_{\mathrm{e}} = 1\,836.152\,673\,6(23)$ [1].

This thesis presents the observation of the transition $(n,l) = (40,36) \rightarrow (41,35)$ of the antiprotonic helium isotope $\overline{\mathrm{p}}^4\mathrm{He}^+$ at a wavelength of $\lambda = 1154.9$ nm (see Figure 1). This transition wavelength is longer than that of any $\overline{\mathrm{p}}\mathrm{He}^+$ resonance studied so far. The transitions in the highly excited $n \geq 40$ region provide important information about the formation process of these atoms, since a laser-induced resonance signal can only be detected if a significant number of $\overline{\mathrm{p}}\mathrm{He}^+$ are formed in the resonance parent state, e.g., $(n,l) = (40,36)$ for the 1154.9 nm transition. Most of the earlier experiments of $\overline{\mathrm{p}}\mathrm{He}^+$ focused on the lower-lying $n \leq 39$ states, while a small fraction of antiprotons occupying some $n = 40$ states have been detected by measuring some other transitions [2,3].

The $\overline{\mathrm{p}}\mathrm{He}^+$ atoms are produced by colliding antiprotons with helium atoms at electronvolt-scale energies,

$$\overline{\mathrm{p}} + \mathrm{He} \rightarrow (\overline{\mathrm{p}}\mathrm{He}^+)_{n,l} + \mathrm{e}^-. \tag{1}$$

Laser spectroscopic studies of various $\overline{\mathrm{p}}\mathrm{He}^+$ transitions have mapped out the distributions of $\overline{\mathrm{p}}\mathrm{He}^+$ occupying the metastable (n,l) states at the formation of the atom [3,4]. These studies have revealed the largest population in the $n = 38$ region. Theoretical studies on the formation of $\overline{\mathrm{p}}\mathrm{He}^+$ have shown that antiprotons are mostly likely captured into $\overline{\mathrm{p}}^4\mathrm{He}^+$ states with principal quantum numbers of around $n_0 = \sqrt{M_{\overline{\mathrm{p}}}^*/m_{\mathrm{e}}} = 38.3$, where $M_{\overline{\mathrm{p}}}^*$ denotes the reduced mass of the $\overline{\mathrm{p}}-^4\mathrm{He}$ system [5]. The formula for n_0 is derived from the assumption that the radius and binding energy of the antiproton are the same

as those of the displaced electron in the $1S$ state. This assumption is supported by the results of the previous experiments described above.

The present experiment was carried out by the ASACUSA (Atomic Spectroscopy and Collisions Using Slow Antiprotons) collaboration at the Antiproton Decelerator (AD) of CERN. The experimental setup was similar to that of Ref. [2]. A pulsed beam containing $(2-3) \times 10^7$ antiprotons with a momentum of 100 MeV/c was extracted from the AD. The $\bar{\mathrm{p}}\mathrm{He}^+$ atoms were produced by stopping the antiprotons in a cryogenic helium gas target [6]. The target contained ^{4}He gas at a temperature of $5-6$ K and a pressure of 60 kPa. A pulsed laser light induced the atomic transition between the metastable state $(40, 36)$ and a state $(41, 35)$ with a short lifetime against Auger emission of the electron (see Figure 1). The $\bar{\mathrm{p}}\mathrm{He}^{2+}$ ions remaining after Auger decay were destroyed by collisions within picoseconds (see the caption of Figure 1). The charged pions emerging from the resulting antiproton annihilations were detected by a Cherenkov counter [7].
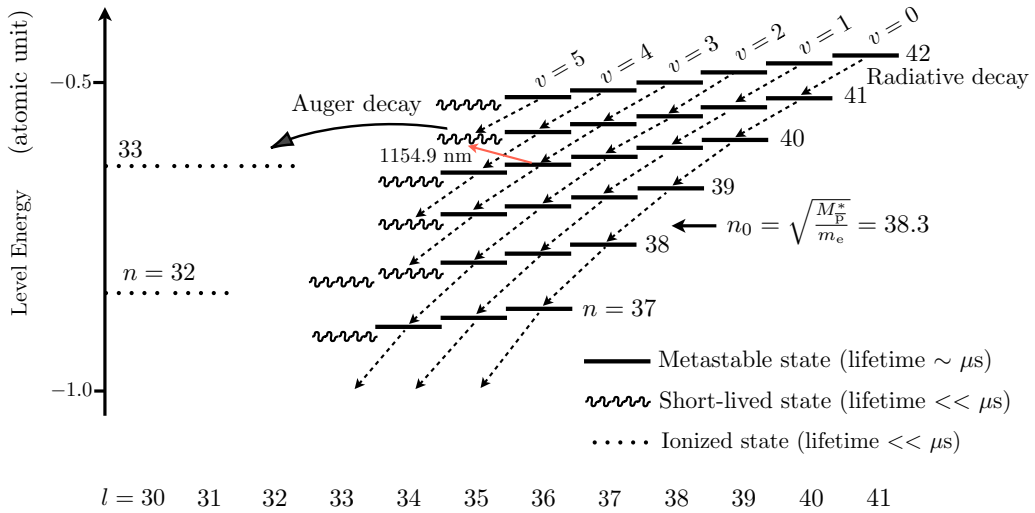

Figure 1: Energy diagram of $\bar{\mathrm{p}}^4\mathrm{He}^+$. The 1154.9 nm transition observed in this work is indicated with a solid red arrow. The ionized l-states with the same n are degenerate so that collisional Stark effects mix the large-l states with the low-l states (the S, P and D states) at large n, resulting in a rapid annihilation of the antiproton in the helium nucleus. Dashed arrows show radiative decays with microsecond-scale lifetimes. $v \equiv n - l - 1$ denotes the vibrational quantum number.

A stimulated first-order Raman scattering process in a H_2 gas cell was utilized to generate a 7 ns long laser pulse with a wavelength of 1154.9 nm, a pulse energy of 4.5 mJ, and a diameter of 2 cm. The pump beam for the Raman process was provided by an injection-seeded titanium sapphire (Ti:Sapphire) laser [8], which produced a light pulse at $\lambda = 780.4$ nm. We passed this beam through a 3 m long Raman gas cell filled with H_2 gas at room temperature and a pressure of 600 kPa. The frequency of the Stokes beam ν_{Stokes} was determined from the relationship $\nu_{\mathrm{Stokes}} = \nu_{\mathrm{Ti:S}} - \nu_{\mathrm{R}}$, where $\nu_{\mathrm{Ti:S}}$ is the frequency of the Ti:Sapphire pump laser and $\nu_{\mathrm{R}} = 124\,570.6 \pm 0.5$ GHz the vibrational $Q(1)$ transition frequency of H_2 [9–11]. For this experiment, no precise calibration [8] was carried out on the reading of the wavelength meter or the Stokes-shifted light, and thus the precision on the transition frequency was limited to around ± 2 GHz which corresponds on a fractional precision of 1×10^{-5}.

Figure 2 (a) shows the resonance profile of the 1154.9 nm transition. This was obtained by plotting the signal intensity of the laser-induced resonant annihilations (see above), averaged over 5 antiproton pulses, as a function of the laser frequency. The resonance profile of $\bar{\mathrm{p}}\mathrm{He}^+$ is known to have the hyperfine splitting which arises from the coupling between the electron spin and the antiproton orbital angular momentum [12]. The data points in Figure 2 (a) were therefore fitted with a two overlapping Lorentzian

functions with a constant offset. The frequency interval between the two Lorentzian functions was fixed to 2 ± 0.5 GHz. We obtained a resonance centroid of $259\,577 \pm 2$ GHz. The experimental uncertainty is mostly due to the uncertainty of the laser wavelength.
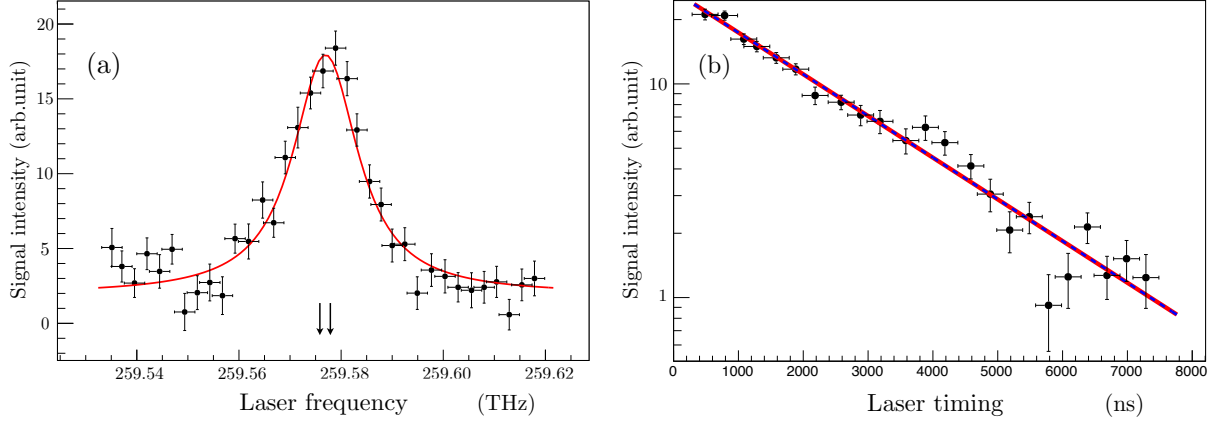

Figure 2: (a) Resonance profile of the $\overline{\text{p}}{}^4\text{He}^+$ transition $(n, l) = (40, 36) \rightarrow (41, 35)$. The solid red curve indicates the best fit of two overlapping Lorentzian functions with a constant offset. The solid arrows show positions of the hyperfine lines. (b) Time evolution of the signal intensity. The origin of the x-axis corresponds to the time at which $\overline{\text{p}}\text{He}^+$ is formed. The frequency of the laser was fixed at the resonance centroid. The solid red line shows the best fit of a single exponential function. The dashed blue line indicates the best fit of a two-level cascade model. Two fit functions overlap each other.

A three-body calculation of Korobov [13] has determined the spin-independent transition frequency of the 1154.9 nm resonance as $259\,591.042$ GHz. This value differed from our experimental frequency measured in the helium target at an atomic density of $n_{\text{He}} = 1.1 \times 10^{21}$ cm^{-3} by -14 GHz. This was assumed to be due to the collisional shift which occurred at the relatively high target densities used in this experiment. The experiment-theory difference was consistent with a collisional shift $\Delta\nu_{\text{col}} = -12$ GHz obtained from the chemical-physics calculations of Bakalov [14].

The full width at half maximum of the resonance profile was 16 ± 5 GHz. This value was larger than the expected value 7 ± 2 GHz which was calculated by numerically solving the optical Bloch equations. The largest contribution to the resonance width arose from power broadening effects. The reason for the difference between the measured and simulated linewidths is not completely understood. Some of the possibilities include an underestimation of collisional broadening effects, the spectral linewidth of the laser, or the natural linewidth.

Figure 2 (b) shows the signal intensity of the 1154.9 nm resonance, against the timing of the laser pulse which was varied between $t = 0.5$ and 8 μs. This corresponds to the time evolution of the population in the state $(40, 36)$, since the signal intensity at each t is proportional to the number of antiprotons occupying that state. The solid red line in Figure 2 (b) indicates the best fit of a single exponential function. The population in the state (40,36) was found to decay with a rate of $\lambda_{(40,36)} = 0.45 \pm 0.04$ μs^{-1}, in which the experimental uncertainty includes the statistical uncertainty and the systematic one due to the uncertainty in the arrival time of the 200-300 ns long antiproton pulse from the AD. The radiative decay rate of the state $(40, 36)$ has been theoretically calculated to be 0.55 μs^{-1} [15] and 0.47 μs^{-1} [13]. The former theoretical value is slightly larger than $\lambda_{(40,36)}$, while the latter in good agreement with $\lambda_{(40,36)}$. This implies that the measured population evolution is well-represented by the intrinsic radiative decay rate of the state $(40, 36)$ and that few metastable atoms exist in states with $n \geq 41$ in the $v = n - l - 1 = 3$ cascade (see Figure 1). The population initially formed in the states $(40, 36)$ and $(41, 37)$ was determined to be respectively $0.06 \pm 0.05\%$ and less than 0.02% of the total number of antiprotons

stopped in the helium target by estimating various backgrounds and efficiencies. This estimation was done using the data of previous experiments [3, 4], a two-level cascade model (see the dashed blue line in Figure 2 (b)), a numerical simulation using the optical Bloch equations, and a Monte Carlo simulation.

The estimated populations in the states $(40, 36)$ and $(41, 37)$ were in agreement with the results of previous experiments which studied the lower-lying state $(39, 35)$ in the $v = 3$ cascade [3, 4]. On the other hand, many theoretical calculations [16] have predicted that a considerable number of $\bar{\text{p}}\text{He}^+$ should be formed in the $n \geq 41$ states. One possibility for the apparent discrepancy between the experimental and theoretical results may be due to the fact that the populations are modified by collisions with helium atoms immediately after the atomic formation, which is not taken into account in the above calculations. The formed $\bar{\text{p}}\text{He}^+$ atoms are assumed to recoil with kinetic energies of several electronvolts, and undergo a rapid thermalization, i.e., they reach a thermal temperature within picoseconds by several collisions. The chemical-physics calculations of Korenman [17], Sauge and Valiron [18] have suggested that most of the highly excited $\bar{\text{p}}\text{He}^+$ atoms are destroyed by collisions during the thermalization stage.

In summary, we have observed the transition $(n, l) = (40, 36) \rightarrow (41, 35)$ of $\bar{\text{p}}^4\text{He}^+$ at $\lambda = 1154.9$ nm. The analysis of the population evolution in the state $(40, 36)$ implies that a relatively small number of atoms are formed in the state $(40, 36)$ and few atoms occupy states with $n \geq 41$ in the $v = 3$ cascade.

References

[1] M. Hori *et al.*, Nature **484**, 475 (2011).

[2] M. Hori *et al.*, Phys. Rev. Lett. **87**, 093401 (2001).

[3] M. Hori *et al.*, Phys. Rev. Lett. **89**, 093401 (2002).

[4] M. Hori *et al.*, Phys. Rev. A **70**, 012504 (2004).

[5] E. Fermi and E. Teller, Phys. Rev. **72**, 399 (1947).

[6] A. Sótér, D. Barna, and M. Hori (in preparation).

[7] M. Hori *et al.*, Nucl. Instrum. Methods Phys. Res. A **496**, 102 (2003).

[8] M. Hori and A. Dax, Opt. Lett. **8**, 1273 (2009).

[9] D. E. Jennings, A. Weber, J. W. Brault, Appl. Opt. **25**, 284 (1986).

[10] W. K. Bischel and M. J. Dyer, Phys. Rev. A **33**, 3113 (1986).

[11] M. J. Dyer and W. K. Bischel, Phys. Rev. A **44**, 3138 (1991).

[12] D. Bakalov and V. I. Korobov, Phys. Rev. A **57**, 1662 (1998).

[13] V. I. Korobov, Phys. Rev. A **77**, 042506 (2008); private communication, (2000/2012).

[14] D. Bakalov *et al.*, Phys. Rev. Lett. **84**, 2350 (2000); private communication, (2013).

[15] P. T. Greenland and R. Thürwächter, Hyperfine Interact. **76**, 355 (1993).

[16] K. Ohtsuki, private communication, (1992). G. Ya. Korenman, Hyperfine Interact. **101 − 102**, 81 (1996); Nucl. Phys. **A692**, 145c (2001). J. S. Cohen, R. L. Martin, and W. R. Wadt, Phys. Rev. A **27**, 1821 (1983). V. K. Dolinov *et al.*, Muon Cat. Fusion **4**, 169 (1989). W. A. Beck, L. Wilets, and M. A. Alberg, Phys. Rev. A **48**, 2779 (1993). J. S. Cohen, Phys. Rev. A **62**, 022512 (2000). K. Tőkési, B. Juhász, and J. Burgdörfer, J. Phys. B: At. Mol. Opt. Phys. **38**, S401 (2005). J. Révai and N. Shevchenko, Eur. Phys. J. D **37**, 83 (2006).

[17] G. Ya. Korenman, Phys. At. Nucl. **59**, 1665 (1996).

[18] S. Sauge and P. Valiron, Chem. Phys. **265**, 47 (2001).